Lithium−Cobalt Citrate Precursors in the Preparation of Intercalation Electrode Materials

E. Zhecheva,[†] R. Stoyanova,[†] M. Gorova,[†] R. Alcántara,[‡] J. Morales,[‡] and J. L. Tirado*,[‡]

Institute of General and Inorganic Chemistry, Bulgarian Academy of Sciences, 1113 Sofia, Bulgaria, and Laboratorio de Química Inorgánica, Facultad de Ciencias, Universidad de Córdoba, Avda. San Alberto Magno s/n, 14004 Córdoba, Spain

Received January 4, 1996. Revised Manuscript Received May 1, 1996[⊗]

Noncrystalline solids with $LiCoC_6H_5O_7 \cdot 5H_2O$ and $(NH_4)_3LiCo(C_6H_5O_7)_2$ compositions were obtained by ethanol dehydration of concentrated lithium−cobalt citrate solutions. Electron spectroscopy of solutions and solid citrates, as well as IR spectroscopy of solid citrates, reveals that in $LiCoC_6H_5O_7 \cdot 5H_2O$ one triionized citrate ion chelates Co^{2+} while two triionized citrate ions surround Co^{2+} in $(NH_4)_3LiCo(C_6H_5O_7)_2$. Lithium−cobalt citrates were used as precursors in the formation of lithium−cobalt mixed oxides. At 400 °C, thermal decomposition of $LiCoC_6H_5O_7 \cdot 5H_2O$ yields a mixture of pseudo-spinel and rhombohedral $LiCoO_2$. From $(NH_4)_3LiCo(C_6H_5O_7)_2$, monophase powders of rhombohedral $LiCoO_2$ were obtained at 400 °C, which consist of hexagonal individual particles with a diameter of 80−120 nm. This product can be annealed up to 800 °C without marked structural changes. The rhombohedral $LiCoO_2$ was used as active cathode material in lithium cells. Cyclic voltammogams showed little changes in the main cathodic and anodic peaks with synthesis temperature. The loss of cell capacity is limited in electrodes prepared at 400 °C from citrate precursors as compared with products of low-temperature synthetic procedures previously reported.

Introduction

The need to develop high-performance positive electrodes in advanced batteries, such as rocking-chair or lithium-ion type cells, has stimulated investigation in two directions. The search of new materials with intercalation/deintercalation behavior has been extended to a vast number of crystalline compounds with different lattice dimensionality. However, success is restricted to one group of layered compounds, Li_xMO_2 (M: Co, Ni), and a three-dimensional spinel structure compound $Li_xMn_2O_4$.[1,2] A second research direction deals with the changes in composition, cation distribution, crystallinity, texture, etc., that can be achieved by changing the synthesis conditions or by different pretreatments of these "standard" compounds.[3−7]

$LiCoO_2$ possesses two structural varieties depending on the preparation conditions. At high temperature (800−900 °C), the solid-state reaction between lithium and cobalt salts yields $LiCoO_2$ (α-$NaFeO_2$ type structure), where lithium and cobalt are ordered to give hexagonal sheets of Li^+ and Co^{3+} in alternate layers.[8,9] During prolonged heating at low temperatures (5−7 days at 400 °C), the interaction between lithium salts and Co_3O_4 leads to the formation of nearly stoichiometric $LiCoO_2$ with pseudo-spinel structure.[10−13] Both structural varieties display different electrochemical properties. In the case of low-temperature $LiCoO_2$, deintercalation/intercalation reactions of Li proceed at lower potential: 3.7/3.5 V for low-temperature $LiCoO_2$ (LT-$LiCoO_2$) and 3.9/3.8 V for high-temperature $LiCoO_2$ (HT-$LiCoO_2$), respectively.[6,10−12,14−17] Besides, the LT-$LiCoO_2$ has lower capacity and worse cyclability than HT-$LiCoO_2$.[10−12]

To prepare low grain size powders of layered $LiCoO_2$ at low temperature (T = 400−600 °C), solution techniques using acetate and glycolate precursors have been reported.[3,19] Recently, Yazami et al.[19] have elaborated a new synthesis method of high surface area $LiCoO_2$ powders, characterized by a layered crystal structure. This method consists in thermal decomposition of the intimate mixture of lithium acetate and cobalt acetate

[†] Bulgarian Academy of Sciences.
[‡] Universidad de Córdoba.
[⊗] Abstract published in *Advance ACS Abstracts,* June 15, 1996.

(1) Ohzuku, T. *Lithium batteries. New Materials, Developments and Perspectives*; Pistoia, G., Ed.; Elsevier Science B.V.: Dordrecht, 1994; p 239.
(2) Thackeray, M. M. *J. Electrochem. Soc.* **1995**, *142*, 2558.
(3) Schleich, D. M. *Solid State Ionics* **1994**, *70−71*, 407.
(4) Pereira-Ramos, J. P. *J. Power Sources* **1995**, *54*, 120.
(5) Rossen, E.; Reimers, J. N.; Dahn, J. R. *Solid State Ionics* **1993**, *62*, 53.
(6) Gummow, R. J.; Thackeray, M. M. *J. Electrochem. Soc.* **1993**, *140*, 3365.
(7) Alcántara, R.; Morales, J.; Tirado, J. L.; Stoyanova, R.; Zhecheva, E. *J. Electrochem. Soc.* **1995**, *142*, 3997.
(8) Johnston, W. D.; Heikes, R. P.; Sestrich, D. *J. Phys. Chem. Solids* **1958**, *7*, 1.
(9) Orman, H. J.; Wiseman, P. J. *Acta Crystallogr.* **1984**, *C40*, 12.
(10) Gummow, R. J.; Thackeray, M. M.; David, W. I. F.; Hull, S. *Mater. Res. Bull.* **1992**, *27*, 327.
(11) Gummow, R. J.; Liles, D. C.; Thackeray, M. M.; David, W. I. F. *Mater. Res. Bull.* **1993**, *28*, 1177.
(12) Rossen, E.; Reimers, J. N.; Dahn, J. R. *Solid State Ionics* **1993**, *62*, 53.
(13) Morales, J.; Stoyanova, R.; Tirado, J. L.; Zhecheva, E. *J. Solid State Chem.* **1994**, *113*, 182.
(14) Nagaura, T.; Nagamine, M.; Tanabe, I.; Miyamoto, N. *Prog. Batt. Sol. Cells* **1989**, *8*, 84.
(15) Nagaura, T.; Tozawa, T. *Prog. Batt. Sol. Cells* **1990**, *9*, 20.
(16) Reimers, J. N.; Dahn, J. R. *J. Electrochem. Soc.* **1992**, *139*, 2091.
(17) Ohzuku, T.; Ueda, A. *J. Electrochem. Soc.* **1994**, *141*, 2972.
(18) Barboux, P.; Tarascon, J. M.; Shokoohi, F. K. *J. Solid State Chem.* **1991**, *94*, 185.
(19) Yazami, R.; Lebrun, N.; Bonneau, M.; Molteni, M. *J. Power Sources* **1995**, *54*, 389.

S0897-4756(96)00009-9 CCC: $12.00

at 550 °C under air for at least 2 h. $LiCoO_2$ thus prepared shows higher performance in terms of rate capacity as compared with the high-temperature analogues. On increasing rate, the decrease in cathode utilization is less marked for LT samples. Thus, LT electrodes show higher capacities than HT electrodes at high rates. This effect has been explained in terms of a quick electrode polarization in HT samples, due to the increased lithium-ion concentration gradient, as a result of the lower active surface area.[19]

The citrate method has been shown to have great potential in the preparation of multicomponent oxides (perovskites, spinels, ferrites, polytitanates, etc.) with a high chemical homogeneity and small particle size.[20−28] Several variants have been elaborated. In the so-called Pechini process,[20] polyhydroxyl alcohols are used to polyesterify the citrate complexes of the metals into a cross-linked polymeric resin, which decomposes above 400 °C.[20,21,24,25] Another method is based on the slight solubility of the citrate salts in ethanol in comparison with water.[26−28] In the citrate gel method, the amorphous citrate precursors are prepared by adding citric acid to a solution of metal salts (usually nitrates) followed by vacuum evaporation.[22,23,29] To our knowledge, there are no data on the formation of lithium cobaltates from citrate precursors.

In aqueous solutions and at equimolar cobalt and citric acid concentrations, citric acid {HOOC−CH_2−C(OH)(COOH)−CH_2−COOH = H_3L} reacts with Co^{2+} to form three types of monomeric complexes: $[CoH_2L]^+$, [CoHL], and $[CoL]^-$. Calculations based on stability constants for cobalt citrate complexes[30] show that $[CoH_2L]^+$ and $[CoL]^-$ occur simultaneously at low pH values, while above pH > 3, complexation of Co^{2+} with triionized citric acid takes place. In the pH range 6−8, $[CoL]^-$ species predominate. In excess of citric acid, the complexation of cobalt with two mols of triionized citric acid $[CoL_2]^{4-}$ takes place which makes an important contribution in the pH range 5−7.[31,32] In concentrated solutions, polynuclear complex formation of Co^{2+} with triionized and quadruply ionized citrate anions starts at pH > 7: $Co_2L(H_{-1}L)^{3-}$ and $Co_2(H_{-1}L)_2^{4-}$.[32] At pH > 5, lithium also forms complexes with the triionized citric acid, whose stability constant is considerably lower than that of the Co analogue: log $K(Li^+ + L^{3-} \rightarrow LiL^{2-})$ = 0.83 and log $K(Co^{2+} + L^{3-} \rightarrow CoL^-)$ = 5.03 for an ionic strength 0.1.[30] From aqueous solutions, cobaltous citrates $Co_3(C_6H_5O_7)_2 \cdot xH_2O$ with x = 2, 4, 10, and 14 are isolated,[33] which, to the best of our knowledge, are not characterized by XRD. Lithium forms monoclinic citrates with the composition $Li_3(C_6H_5O_7) \cdot xH_2O$ (x = 2, 5) and $Li(C_6H_7O_7) \cdot xH_2O$ (x = 0, 1).[34−36]

In the present work we propose a new method for the preparation of ultrafine layered $LiCoO_2$ by thermal decomposition of homogeneous lithium cobalt citrate precursors.

Experimental Section

By variation of the Li:Co:citric acid ratio, as well as the pH value of the Li−Co citrate solution, lithium cobalt citrates with different compositions were prepared. A Li−Co citrate precursor with Li:Co:citric acid = 1:1:1 or 1:1:2 was synthesized according to the following preparation procedure: solid Li_2CO_3 (A.R. Merck) was added to a 75% solution of $Co(NO_3)_2 \cdot 6H_2O$ (A.R. Merck). A saturated solution of citric acid (Co:citric acid = 1:1 or 1:2) was added dropwise to this mixture with intensive stirring, until a clear solution was obtained. The pH value was adjusted to 7 with ammonia and then the Li−Co citrate solution was heated at 80 °C to complete the reaction. This solution was cooled to room temperature and ethanol dehydrated. The precipitate thus obtained was filtered, washed with ethanol, and dried at 100 °C in air. For comparison, pure cobalt citrates were also isolated by ethanol dehydration of concentrated 3:2 and 1:2 Co:H_3L solutions.

The lithium content of the samples was determined by atomic absorption analysis. The total amount of cobalt was determined complexometrically and by atomic absorption analysis. The citrate complexes were analyzed according to the standard procedures for C and H (as CO_2 and H_2O) and for N by the Dumas method. The mean oxidation state of cobalt was determined by iodometric titration.

The X-ray phase analysis was performed with a Philips diffractometer using Cu Kα radiation. Infrared spectra were recorded on a Specord-75 (ex-GDR) spectrometer in KBr pellets or in nujol mulls in the 4000−400 cm^{-1} range. The specific surface area of the samples was determined by the BET method using low-temperature nitrogen adsorption.

Electronic absorption spectra and diffuse reflectance spectra were carried out at room temperature on a UV−vis spectrometer (Carl-Zeiss). Absorption spectra of diluted solutions (0.003 M) were recorded with 50 mm quartz cells, while 1 mm cells were used to collect the spectra of the concentrated solutions (0.65 M).

TG and DTA measurements were performed with a Paulik-Paulik-Erdey (MOM, Hungary) apparatus in air and samples weighting 150 mg each were used. DSC measurements were carried out on Perkin-Elmer apparatus in nitrogen and in air with a heating rate of 10 °C min and samples weighting 1.5 mg each were used.

The EPR spectra were registered as the first derivative of the absorption signal with an ERS-220/Q spectrometer (ex-GDR) within the temperature range between 90 and 400 K. The g factors were established with respect to a Mn^{2+}/ZnS standard. The signal intensity was determined by double integration of the experimental EPR spectrum.

Transmission electron microscopy and electron diffraction measurements were made on a JEOL-100B instrument with 80 kV accelerating voltage. SEM analysis on powder samples coated with gold were carried out in a JEOL-5300 instrument with 15 and 25 kV accelerating voltage.

Electrochemical experiments were carried out in two-electrode Li/$LiClO_4$(PC:EC)/$LiCoO_2$ cells. Electrodes using oxide samples as active material were prepared as 7 mm diameter pellets by pressing at 200 MPa a mixture of 80% of

(20) Pechini, M. U.S. Patent 3,330,697, **1967**.
(21) Hennings, D.; Mayr, W. *J. Solid State Chem.* **1978**, *26*, 329.
(22) Anderton, D. J.; Sale, F. R. *Powder Metall.* **1979**, *22*, 14.
(23) Baythoun, M. S. G.; Sale, F. R. *J. Mater. Sci.* **1982**, *17*, 2757.
(24) Douy, A.; Odier, M. *Mater. Res. Bull.* **1989**, *24*, 1119.
(25) Choy, J.-H.; Han, Y.-S.; Kim, J.-T.; Kim, Y.-H. *J. Mater. Chem.* **1995**, *5*, 57.
(26) Sankaranarayanan, V. K.; Pankhurst, Q. A.; Disckon, D. P. E.; Johnson, C. E. *J. Magn. Magn. Mater.* **1993**, *120*, 73.
(27) Sankaranarayanan, V. K.; Pankhurst, Q. A.; Disckon, D. P. E.; Johnson, C. E. *J. Magn. Magn. Mater.* **1993**, *125*, 199.
(28) Sankaranarayanan, V. K.; Pankhurst, Q. A.; Disckon, D. P. E.; Johnson, C. E. *J. Magn. Magn. Mater.* **1994**, *130*, 288.
(29) Chu, C. T.; Dunn, B. *J. Am. Ceram. Soc.* **1987**, *70*, C375.
(30) Martell, A. E.; Smith, R. M. *Critical Stability Constants*; Plenum Press: New York, 1977; Vol. 3, p 161.
(31) Li, N. C.; White, J. M. *J. Inorg. Nucl. Chem.* **1960**, *16*, 131.
(32) Salnikov, Yu. I.; Saprikova, Z. A. *Koord. Khim.* **1984**, *10*, 887 (in Russian).
(33) *Gmelins Handbuch der Anorganischen Chimie*; Verlag-Chimie GMBH: Berlin, 1932, Vol. 58; Teil A.
(34) Glusker, J. P.; van der Helm, D.; Love, W. E.; Dornberg, M. L.; Minkin, J. A.; Johnson, C. K.; Patterson, A. L. *Acta Crystallogr.* **1965**, *19*, 561.
(35) Rossi, M.; Rickles, L. F.; Glusker, J. P. *Acta Crystallogr.* **1983**, *C39*, 987.
(36) Schudt, E., Weitz, III/5a, G., Landolt-Bornstein, *Structure Data on Organic Crystals C...C_{13}*; Hellwege, K.-H., Hellwege, A. M., Eds.; Springer-Verlag: Berlin, 1971.

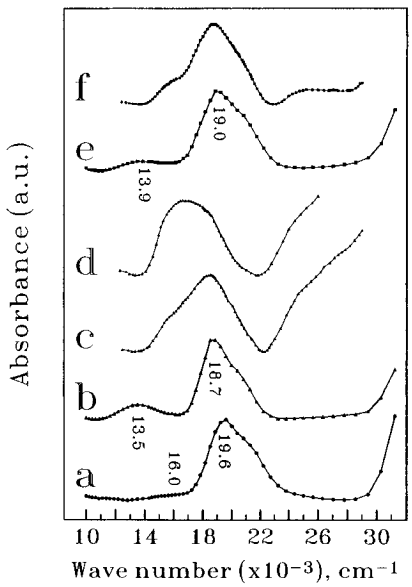

Figure 1. Absorption spectra of cobalt nitrate−citric acid solutions at pH = 7: (a) $Co(H_2O)_6^{2+}$; (b) cobalt/citrate 1:1, [Co] = 0.65 M, path length 1 mm; (c) cobalt/citrate 1:1, [Co] = 0.003 M, path length 50 mm, the spectrum was recorded after 1 hour of the dilution of solution (b); (d) cobalt/citrate 1:1, [Co] = 0.003 M, path length 50 mm, the spectrum was recorded after 30 h of the dilution of solution (b); (e) cobalt/citrate 1:2, [Co] = 0.65 M, path length 1 mm; (f) cobalt/citrate 1:2, [Co] = 0.003 M, path length 50 mm, the spectrum was recorded after 30 h of the dilution of solution (e).

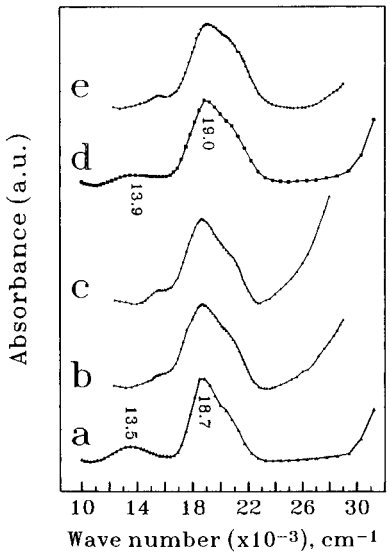

Figure 2. Absorption spectra of lithium−cobalt citric acid solutions at pH = 7: (a) cobalt/citrate 1:1, [Co] = 0.65 M, path length 1 mm; (b) cobalt/citrate 1:1, [Co] = 0.003 M, path length 50 mm, the spectrum was recorded after 1 h of the dilution of solution (a); (c) cobalt/citrate 1:1, [Co] = 0.003 M, path length 50 mm, the spectrum was recorded after 30 h of the dilution of solution (a); (d) cobalt/citrate 1:2, [Co] = 0.65 M, path length 1 mm; (e) cobalt/citrate 1:2, [Co] = 0.003 M, path length 50 mm, the spectrum was recorded after 30 h of the dilution of solution (d).

sample (ca. 12 mg) and 8% of ethylene/propylene/diene monomers (EPDM) terpolymer (Aldrich) and 12% carbon black (Strem 4N) to improve the mechanical and electronic conduction properties. Lithium electrodes consisted in a clean 7 mm diameter lithium metal disk. The electrolyte solution (1 M $LiClO_4$ in a 1:1 mixture of bidistilled propylene carbonate (PC) and ethylene carbonate (EC) Merck) was supported by porous glass−paper disks. All cell manipulations were carried out inside the glovebox (M. Braun) under argon atmosphere (water content < 2 ppm). The electrochemical measurements were obtained by a multichannel system MacPile alternatively working under potentiostatic and galvanostatic conditions. Prior to the potentiostatic experiments the cells were allowed to relax until the condition $\Delta V/\Delta t < 1$ mV/h was fulfilled. Step potential electrochemical spectroscopy (SPES) was carried out by using 10 mV steps. Current relaxation was recorded during 1 h at each step. Continuous galvanostatic cycling was performed at C/50, i.e., at a constant current that could reach $\Delta x = 1$ in Li_xCoO_2 in 50 h.

Results and Discussion

Lithium Cobalt Citrate Precursors. The complex formation at pH = 7 in concentrated solutions of Li−Co citrates was followed by the systematic changes in the electronic absorption spectra of Co^{2+} (Figure 1). Some important features of the solution spectra are considered: (i) the changes in the position of the absorption bands relative to those of the cobalt−aqua complex; (ii) the effect of the dilution on the absorption spectra; (iii) the dependence of the position of the absorption bands on the cobalt/citric acid ratio. In the visible spectral range, the absorption spectrum of the Co−aqua complex $Co(H_2O)_6^{2+}$ displays one intense band at 19 600 cm^{-1} and a shoulder at about 16 000 cm^{-1}. According to the crystal field theory, these bands can be ascribed to the d−d transitions for Co^{2+} in a field with octahedral symmetry:[37] $\nu_3(^4T_{1g}(P)-{}^4T_{1g}) = 19\,600$ cm^{-1} and ν_2-$(^4A_{2g}-{}^4T_{1g}) \cong 16\,000$ cm^{-1} (Figure 1a). At pH = 7, the addition of equimolar amounts of citric acid to the concentrated solution of $Co(NO_3)_2$ results in a shift of the two absorption bands towards the lower energies: $\nu_3 = 18\,700$ cm^{-1} and $\nu_2 = 13\,500$ cm^{-1} (Figure 1b). This indicates the cobalt−citrate complex formation in concentrated cobalt-citrate solutions (Co:H_3L = 1:1). After dilution, the two absorption bands merge gradually into one broad band at about 15 000 cm^{-1}, indicating d−d transitions of a pseudotetrahedrally coordinated Co^{2+} (Figure 1c,d).[37] The reduction in the coordination number of Co^{2+} in diluted cobalt−citrate solutions can be explained in terms of an equilibrium among polynuclear and monomeric cobalt−citrate complexes. This result is very interesting taking into account that Fe(II) and Ni(II) citrate(3−) complexes are monomeric even in aqueous solutions with high ionic strengths.[38] When Co:H_3L ratio is changed from 1:1 to 1:2, the absorption spectrum of Co^{2+} is altered: the ν_2 and ν_3 bands are shifted to the higher energies in comparison to that of the 1:1 cobalt−citrate complex, but they remain red shifted relative to the Co−aqua complex (Figure 1e). In contrast to the 1:1 cobalt−citric acid solution, the absorption spectrum of the diluted 1:2 solution displays the typical features of an octahedrally coordinated Co^{2+} (Figure 1f). These results point to the complexation of Co^{2+} with two citrate ions in diluted and concentrated 1:2 solutions. For the concentrated 1:1 and 1:2 solutions, the presence of Li^+ ions does not affect the absorption spectrum of Co^{2+} (Figure 2a,d). However, lithium ions stabilize the polynuclear 1:1 cobalt citrate complexes, as was demonstrated by the retention of the octahedral coordination of Co^{2+} after dilution (Figure 2b,c).

(37) Lever, A. B. P. *Inorganic Electron Spectroscopy*, Elsevier, **1984**.
(38) Strouse, J. *J. Am. Chem. Soc.* **1977**, *99*, 572.

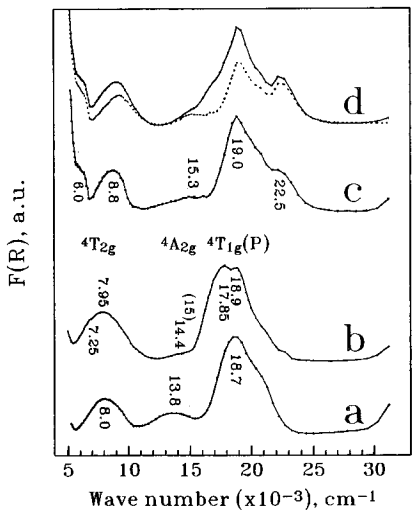

Figure 3. Diffuse reflectance spectra of solid citrates: (a) $LiCo(C_6H_5O_7)\cdot 5H_2O$; (b) $Co[Co(C_6H_5O_7)]_2\cdot 4H_2O$; (c) $(NH_4)_3LiCo(C_6H_5O_7)_2$; (d) mixture of $(NH_4)_4Co(C_6H_5O_7)_2$ and $Co[Co(C_6H_5O_7)]_2\cdot 4H_2O$ (85/15 wt %). The dotted curve is the residual spectrum obtained after substraction of the spectrum (b) from the spectrum (d).

Ethanol dehydration of the concentrated lithium−cobalt−citrate solutions with Co:H_3L = 1:1 and 1:2 yields violet and pink precipitates with a Co:H_3L ratio equal to that in the solution. Elemental analysis of the complexes gave Li = 2.03%, Co = 17.18%, C = 20.7%, H = 4.44%, and Li = 1.42%, Co = 11.90%, C = 28.66%, H = 5.07% N = 9.56%, which agree well with the calculated values for $LiCoC_6H_5O_7\cdot 5H_2O$ (Li = 2.01%, Co = 17.09%, C = 20.88%, H = 4.35%) and $(NH_4)_3LiCo(C_6H_5O_7)_2$ (Li = 1.39%, Co = 11.84%, C = 28.92%, H = 4.42%, and N = 8.44%), respectively. Both precipitates are XRD amorphous and hygroscopic.

Diffuse reflectance spectroscopy reveals some important characteristics for the Co^{2+} coordination in the amorphous lithium−cobalt citrates. For $LiCoC_6H_5O_7\cdot 5H_2O$, the comparison of diffuse reflectance spectrum of the precipitate with the absorption spectrum of the solution shows that the octahedral coordination of Co^{2+} in the solid citrate is the same as in the polynuclear 1:1 cobalt−citrate complex formed in the concentrated solution (Figure 3a): $\nu_1(^4T_{2g}-{}^4T_{1g}) = 8000$, $\nu_2(^4A_{2g}-{}^4T_{1g}) = 13\,600$, $\nu_3(^4T_{1g}(P)-{}^4T_{1g}) = 18\,700$ cm^{-1}. Within the framework of the crystal field theory, one may estimate the strength of the crystal field and Racah's parameters for Co^{2+}: D_q = 790 cm^{-1}, B = 860 cm^{-1}. As a comparison, for $Co(H_2O)_6^{2+}$ these parameters are D_q = 920 and B = 850 cm^{-1}.[37] The reduction in the crystal field strength for Co^{2+} in the citrate salt shows unambiguously that one citrate ion chelates to one Co^{2+}. For pure $Co[CoC_6H_5O_7]_2\cdot 4H_2O$, the reflectance spectrum consists of two intense bands at 17 850 and 18 900 cm^{-1}, as well as of three less intense bands at 14 500, 7900, and 7200 cm^{-1} (Figure 3b). These electronic transitions can be attributed to two kinds of Co^{2+} ions: one of them is in a weaker crystal field (ν_1 = 7250, ν_2 = 14 400, and ν_3 = 17 850 cm^{-1}), and the other is in a crystal field close to that of Co^{2+} in the 1:1 cobalt citrate complex (ν_1 = 7950, ν_2 = 15 000, and ν_3 = 18 900 cm^{-1}). The difference in the diffuse reflectance spectra of pure $Co[CoC_6H_5O_7]_2\cdot 4H_2O$ and $LiCoC_6H_5O_7\cdot 5H_2O$ shows that a mixed lithium−cobalt citrate is isolated by ethanol dehydration of a concentrated lithium−cobalt citrate solution (for Co:H_3L = 1:1). This means that lithium ions act as counterions in the solid precipitate $LiCoC_6H_5O_7\cdot 5H_2O$. For $(NH_4)_3LiCo(C_6H_5O_7)_2$ with a lower Co:H_3L ratio (Co:H_3L = 1:2), Co^{2+} ions are in a tetragonally distorted octahedral field which is demonstrated by the splitting of ν_1 and ν_3 absorption bands: 6000 and 8800; 15 300, 19 000 and 22 500 cm^{-1} (Figure 3c). The same coordination of Co^{2+} ions is observed for pure Co analogue, which contains $(NH_4)_4Co(C_6H_5O_7)_2$ and $Co[CoC_6H_5O_7]_2\cdot 4H_2O$ in a ratio of 85:15 wt % (Figure 3d). Thus, one may conclude that one and two citrate ions chelate to the Co^{2+} ion in $LiCoC_6H_5O_7\cdot 6H_2O$ and $(NH_4)_3LiCo(C_6H_5O_7)_2$, respectively, and determine the different symmetry and strength of the crystal field for Co^{2+} in both cases.

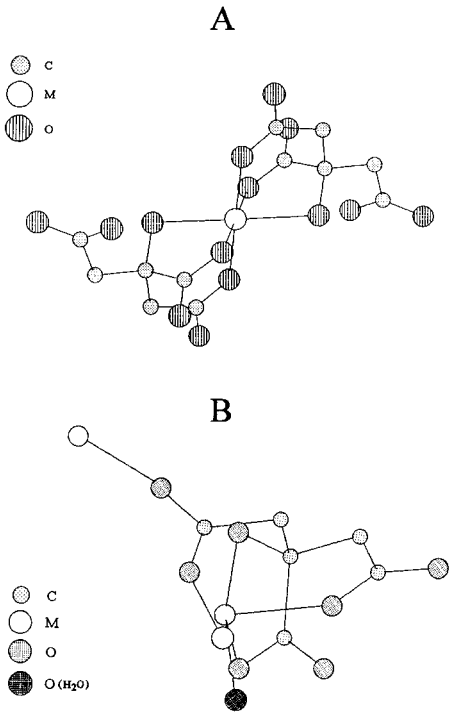

Figure 4. Schematic representation of the chelation in $(NH_4)_4M(C_6H_5O_7)_2$ (A) and $[M(H_2O)_6][M(C_6H_5O_7)(H_2O)]_2\cdot 2H_2O$ (B). Structural data are taken from refs 39 and 40, and 41−43, respectively.

Ammonium metal citrates with the composition $(NH_4)_4M(C_6H_5O_7)_2$ are known only for Zn and Cu.[39,40] X-ray single-crystal diffraction data show that two triionized discrete citrate ions complete a tetragonally distorted octahedral coordination around the metal ion (Figure 4A). The intermolecular association is achieved by ammonium counterions. Each ligand acts as a tridentate chelate, in which the protonated hydroxyl group, one oxygen from the terminal carboxyl group and one oxygen from the central carboxyl group are coordinated to the metal ion (Figure 4A). The M−O (hydroxyl) bonds are longer relative to the M−O (carboxyl) bonds. For 1:1 metal citrate(3−) complexes, a tridentate chelation is also established in the crystal structure of iron and manganous citrate salts with the composition $[M(H_2O)_6][M(C_6H_5O_7)(H_2O)]_2\cdot 2H_2O$ (Figure 4B).[41−43] For

(39) Swanson, R.; Ilsey, W. H.; Stanislowski, A. G. *J. Inorg. Biochem.* **1983**, *18*, 187.
(40) Bott, R. C.; Sagatys, D. S.; Lynch, D. E.; Smith, G.; Kennard, C. H. L.; Mak, T. C. W. *Aust. J. Chem.* **1991**, *44*, 1495.
(41) Carrell, H. L.; Glusker, J. P. *Acta Crystallogr.* **1973**, *B29*, 638.
(42) Glusker, J. P.; Carrell, H. L. *J. Mol. Struct.* **1973**, *15*, 151.

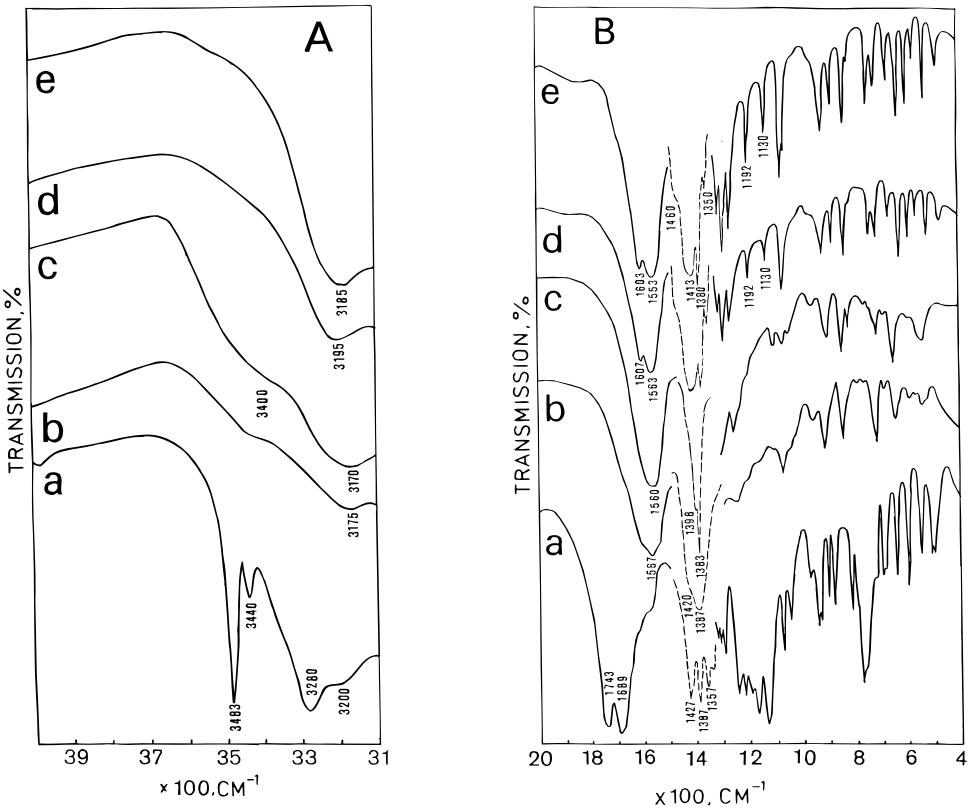

Figure 5. IR spectra in the range 4000−3000 cm^{-1} (A) and 2000−400 cm^{-1} (B) for (a) citric acid, $C_6H_8O_7 \cdot H_2O$; (b) $LiCo(C_6H_5O_7) \cdot 5H_2O$; (c) $Co[Co(C_6H_5O_7)]_2 \cdot 4H_2O$; (d) $(NH_4)_3LiCo(C_6H_5O_7)_2$; (e) mixture of $(NH_4)_4Co(C_6H_5O_7)_2$ and $Co[Co(C_6H_5O_7)]_2 \cdot 4H_2O$ (85/15 wt %). The spectra were recorded with nujol mulls except for the spectral range 1500−1300 cm^{-1} where KBr pellets are used.

these compounds, one triionized citrate ion forms the tridentate chelate, whereas both oxygen atoms from the other terminal carboxylate group bridge two other metal ions (Figure 4B).

Further information about the citrate ligands can be obtained from the IR spectra of the lithium−cobalt citrate salts. Figure 5 compares the IR spectra of citric acid ($C_6H_8O_7 \cdot H_2O$) and Li−Co citrate salts. In the spectral range of the stretching vibrations of OH, the narrow bands at 3480 and 3440 cm^{-1} and the broad bands at 3280 and 3210 cm^{-1} reveal the formation of a complex network of hydrogen bonding in the citric acid (Figure 5A). The spectra of the citrate salts show one diffuse band at near 3180 cm^{-1}, which can be assigned to a protonated hydroxyl group. Furthermore, the bands in the 1380−1350 and 1190−1100 cm^{-1} spectral ranges most probably correspond to the bending and stretching vibrations of OH and C−O(H) for tertiary alcohols (Figure 5B). The broad band at about 3400 cm^{-1} can be attributed to the crystal and/or coordination water for $LiCo(C_6H_5O_7) \cdot 5H_2O$ and $Co[Co(C_6H_5O_7)]_2 \cdot 4H_2O$ (Figure 5A). The conversion of citric acid into citrate salts is demonstrated by the replacement of the five characteristic vibrations of −COOH, corresponding to $\nu_{C=O}$ = 1740 and 1690 cm^{-1}; δ_{OH}(in-plane) = 1420 cm^{-1}, ν_{C-O} 1300−1200 cm^{-1} and δ_{OH}(out-of-plane) = 930 cm^{-1}, by two characteristic vibrations of $-CO_2^-$, corresponding to the antisymmetric and symmetric stretching vibrations (ν_{as} and ν_s) near 1570 and 1410 cm^{-1}, respectively (Figure 5B). This means that for all citrates investigated, a triionized citrate ion $\{OOC-CH_2-C(OH)(COO)-CH_2-COO\}^{3-}$ surrounds the Co^{2+} ion. In addition, for $(NH_4)_3LiCo$ and $(NH_4)_4Co$ citrates, the antisymmetric mode is split, whereas the vibrations of $-CH_2$ and NH_4 groups (about 1460 cm^{-1}) may also contribute to the complex structure of the symmetric mode (Figure 5B).

From many experimental results on IR spectra of carboxylate salts, it has been established that the trends in position of and separation between the antisymmetric and symmetric stretching vibrations of $-CO_2^-$ can be used as a criterion for the mode of carboxylate coordination around the metal ions.[44−46] In the case of strong intra- and intermolecular hydrogen bonding, an empirical correlation between the position of the symmetric vibration and the carboxylate coordination has been proposed: values of $\nu(OCO)_s$ greater than 1414 cm^{-1} point to bridging carboxylate, while values in the 1414−1400 cm^{-1} spectral range and those lower than 1400 cm^{-1} indicate monodentate and bidentate carboxylate, respectively.[44,46] The ν_{as} and ν_s frequencies for the samples investigated are given in Table 1. For comparison, Table 1 also contains data on the values of ν_{as} and ν_s for lithium and nickel acetates where bridging and monodentate coordination of the $-CO_2^-$ groups has been found, respectively.[47,48] Having in mind the single-crystal data on 1:1 and 1:2 citrates (Figure 4), the values

(43) Strouse, J.; Layten, S. W.; Strouse, C. E. *J. Am. Chem. Soc.* **1977**, *99*, 562.

(44) Catterick, J.; Thornton, P. *Adv. Inorg. Chem. Radiochem.* **1977**, *20*, 291.

(45) Deacon, G. B.; Philips, R. J. *Coord. Chem. Rev.* **1980**, *33*, 227.

(46) Battaglia, L. P.; Corradi, A. B.; Marcotrigiano, G.; Menabue, L.; Pellacanni, G. C. *J. Am. Chem. Soc.* **1980**, *102*, 2663.

(47) Cadene, M.; Vergnoux, A. M. *Spectrochim. Acta* **1972**, *A28*, 1663.

(48) Curtis, N. F. *J. Chem. Soc. A* **1968**, 1579.

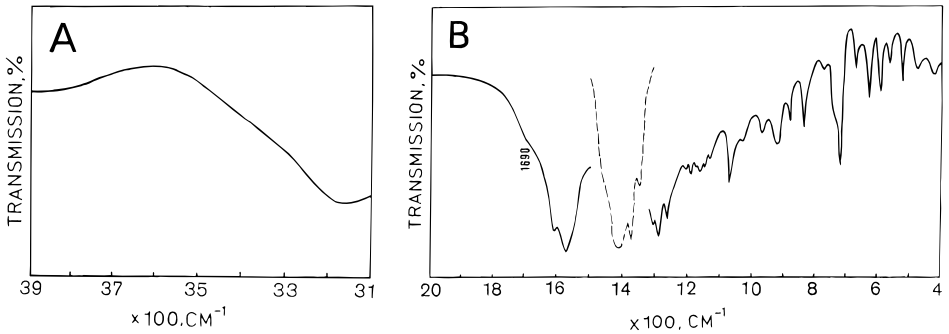

Figure 6. IR spectra in the range 4000−3000 cm^{-1} (A) and 2000−400 cm^{-1} (B) for $(NH_4)_3LiCo(C_6H_5O_7)_2$ heated at 165 °C for 4 h. The spectra were recorded with Nujol mulls except for the spectral range 1500−1300 cm^{-1} where KBr pellets are used.

Table 1. Carboxylate Stretching Frequencies in Citrate Salts

compound	antisym str $\nu(OCO)_{as}$, cm^{-1}	sym str $\nu(OCO)_s$, cm^{-1}
$LiCo(C_6H_5O_7)\cdot 5H_2O$	1567	1420
$Co[Co(C_6H_5O_7)]_2\cdot 4H_2O$	1560	1398
$(NH_4)_3LiCo(C_6H_5O_7)_2$	1607	(1460)?
	1563	1413
$(NH_4)_4Co(C_6H_5O_7)_2$ +	1603	(1460)?
$Co[Co(C_6H_5O_7)]_2\cdot$ $4H_2O$ (85/15 wt %)	1553	1413

of the symmetric modes of all the citrates investigated (Table 1) can be interpreted as monodentate carboxylates.

The above results throw further light on the structure of Co^{2+}−citrate(3−) complexes in diluted and concentrated solutions. For diluted 1:1 solutions, the tridentate chelate and one water molecule form the tetrahedral coordination of Co^{2+} in the monomeric $[CoL]^-$ complex. For concentrated 1:1 solutions, the participation of two additional oxygen atoms from two other citrate ions in the coordination sphere of Co^{2+} (terminal carboxylate groups not involved in the chelation) would bind the monomeric $[CoL]^-$ complexes into a polynuclear complex. Finally, in excess of citric acid, monomeric $[CoL_2]^{4-}$ species dominate in concentrated and diluted solutions where two citrate ions are tridentate chelated to one Co^{2+} ion.

Ammonium−lithium−cobalt citrate and lithium−cobalt citrate are thermally unstable. Above 140 °C $(NH_4)_3LiCo(C_6H_5O_7)_2$ partially transforms into its acid analogue, $(NH_4)_{3-x}H_xLiCo(C_6H_5O_7)_2$, which is manifested by the appearance of the −COOH stretching frequency at 1690 cm^{-1} (Figure 6). Between 140 and 290 °C, one endothermic peak, depending slightly on the heating rate, and the corresponding weight loss are observed in the DTA and TG curves (Figure 7). This endothermic peak reflect the NH_3 evolution, as well as the dehydration of citrate into aconitate ($C_6H_5O_7^{3-}$ to $C_6H_3O_6^{3-}$) as it was observed for other citrate salts.[21] The undecomposed residual organics burns out explosively above 300 °C. The temperature range where the combustion process takes place depends strongly on the heating rate (Figure 7). Lithium−cobalt citrate, $LiCo(C_6H_5O_7)\cdot 5H_2O$, displays different thermochemical properties (Figure 8): in the temperature ranges 100−200 and 200−230 °C, DTA and TG curves show two endothermic peaks with the corresponding weight loss and reveal dehydration of free water and transformation into aconitate, respectively. Between 250−290 and 290−330 °C, two exothermic processes take place, followed, above 350 °C, by a strong exothermic process with drastic

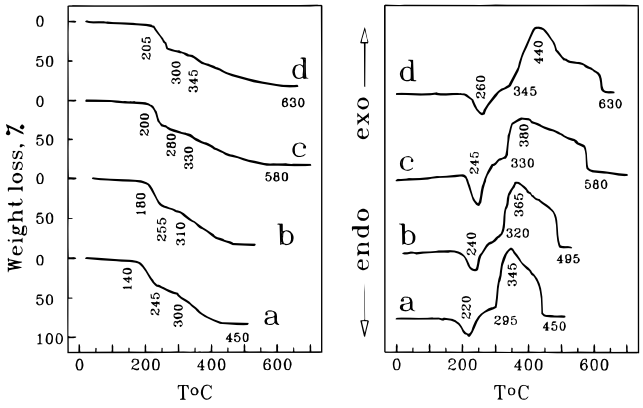

Figure 7. TG and DTA curves of $(NH_4)_3LiCo(C_6H_5O_7)_2$ as a function of heating rate: (a) 2, (b) 3.5, (c) 5, and (d) 10 °C/min.

weight loss due to the vigorous combustion reactions of the residual organics. Final weight losses for $(NH_4)_3LiCo(C_6H_5O_7)_2$ and $LiCo(C_6H_5O_7)\cdot 5H_2O$ are 82.78% and 71.52%, respectively, which agree with the calculated values for a final product $LiCoO_2$: 80.36% and 71.63%.

The formation of mixed lithium−cobalt citrates with the composition Li:Co:citrate = 1:1:1 and 1:1:2 is clearly visible in the DSC curves (Figure 9). Irrespective of the gas atmosphere (nitrogen or air), all curves display one endothermic peak between 150 and 250 °C which corresponds to the dehydration process. The effect of lithium is manifested by the shift of the endothermic peak toward higher temperatures (Figure 9). The second step of thermal decomposition depends on the atmosphere: under nitrogen, an endothermic decomposition takes place above 360 °C, while in air, a strong exothermic decomposition/oxidation is developed. These processes occur at different temperatures, depending both on lithium content and on Co/citrate ratio (Figure 9).

Ultrafine $LiCoO_2$. At 400 °C and with low heating rate (1 °C/min), thermal decomposition of both citrate precursors yields lithium−cobalt oxides with the same Li/Co ratio as in the initial compositions. Figure 10 shows the XRD patterns of $LiCoO_2$, obtained at 400 °C from the citrate salts with Li:Co:Cit = 1:1:1 and 1:1:2, respectively. For comparison, the XRD pattern of LT-$LiCoO_2$, obtained by solid-state reaction between LiOH and Co_3O_4 at 450 °C during 7 days, is also given.[13] The good separation between (108) and (110) diffraction lines, as well as between (006) and (102) diffraction lines, shows that $LiCoO_2$, obtained from $(NH_4)_3LiCo(C_6H_5O_7)_2$ at 400 °C, has a structure different from the

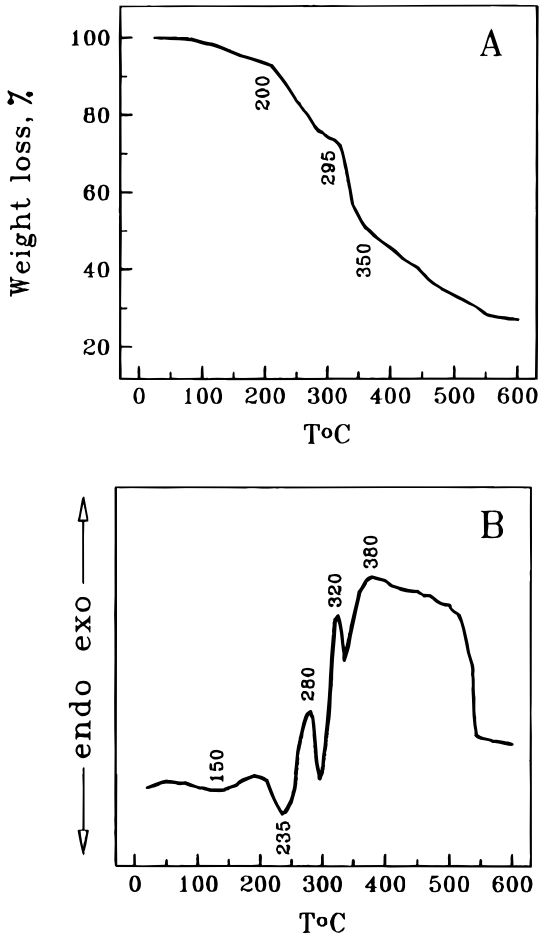

Figure 8. TG and DTA curves of $LiCo(C_6H_5O_7)\cdot 5H_2O$; heating rate 3.5 °C/min.

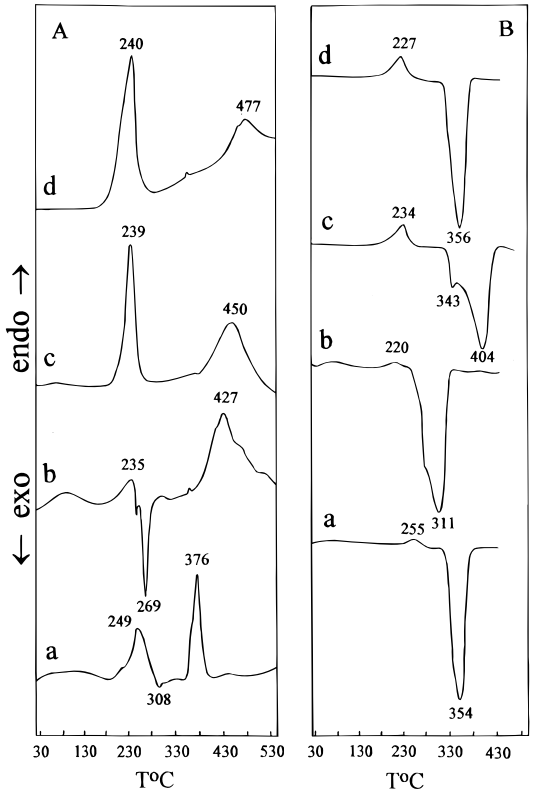

Figure 9. DSC curves under nitrogen (A) and in air (B) for (a) $LiCo(C_6H_5O_7)\cdot 5H_2O$; (b) $Co[Co(C_6H_5O_7)]_2\cdot 4H_2O$; (c) $(NH_4)_3LiCo(C_6H_5O_7)_2$; (d) mixture of $(NH_4)_4Co(C_6H_5O_7)_2$ and $Co[Co(C_6H_5O_7)]_2\cdot 4H_2O$ (85/15 wt %).

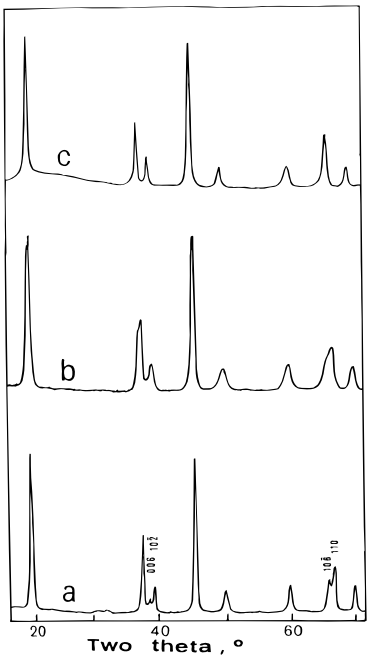

Figure 10. XRD patterns of $LiCoO_2$ obtained at 400 °C for 20 h from $(NH_4)_3LiCo(C_6H_5O_7)_2$ (a) and $LiCo(C_6H_5O_7)\cdot 5H_2O$ (b). For comparison, the XRD pattern of pseudo-spinel $LiCoO_2$ (c), obtained by solid-state reaction between LiOH and Co_3O_4 at 450 °C for 7 days is also shown.

pseudo-spinel structure of LT-$LiCoO_2$ and close to the "ideal" trigonal α-$NaFeO_2$ type structure. Ex-citrate $LiCoO_2$ exhibits a high ratio of the unit cell parameters $c/a = 4.97$, which is typical for HT-$LiCoO_2$. The splitting of the (003) diffraction line indicates that, at 400 °C, the thermal decomposition product of $LiCo(C_6H_5O_7)\cdot 5H_2O$ consists of two $LiCoO_2$ phases which are characterized by a pseudo-spinel and trigonal structure, respectively (Figure 10). The formation of monophase and diphase products from the two types of citrates at 400 °C is probably related to the different mechanism of their thermal decomposition (Figures 7−9).

TEM investigations show that monophase $LiCoO_2$, obtained from the citric salt with Li:Co:Cit = 1:1:2 at 400 °C, consist of hexagonal individual particles with a diameter of 80−120 nm (Figure 11). Assuming spherical geometry, the crystal size, estimated from the specific surface area, is about 110 nm, which is consistent with that determined from TEM observations. This indicates that ex-citrate $LiCoO_2$ powders calcined at 400 °C are composed of nonagglomerated ultrafine particles. Further calcination of ex-citrate $LiCoO_2$ results both in crystal growth and particle roundness (Figures 11 and 12). At 800 °C, uniformly sintered grains of 2−3 μm are formed (Figure 12). It is important to note that high-temperature ex-citrate $LiCoO_2$ shows a relatively narrow crystal size distribution (Figure 12). For sake of comparison, Figure 12 also shows the SEM pictures of $LiCoO_2$ obtained by solid-state reaction between LiOH and Co_3O_4 at 800 °C for 24 h, where well-crystallized platelike particles with a relatively broad crystal size distribution (0.5−3 μm) are observed. It must be emphasized that the changes in morphology of ex-citrate $LiCoO_2$ during calcination proceed with the preservation of the trigonal crystal structure (Table 2).

IR spectroscopy of lithium transition metal oxides reveals the separate vibrations of the LiO_2 and MO_2

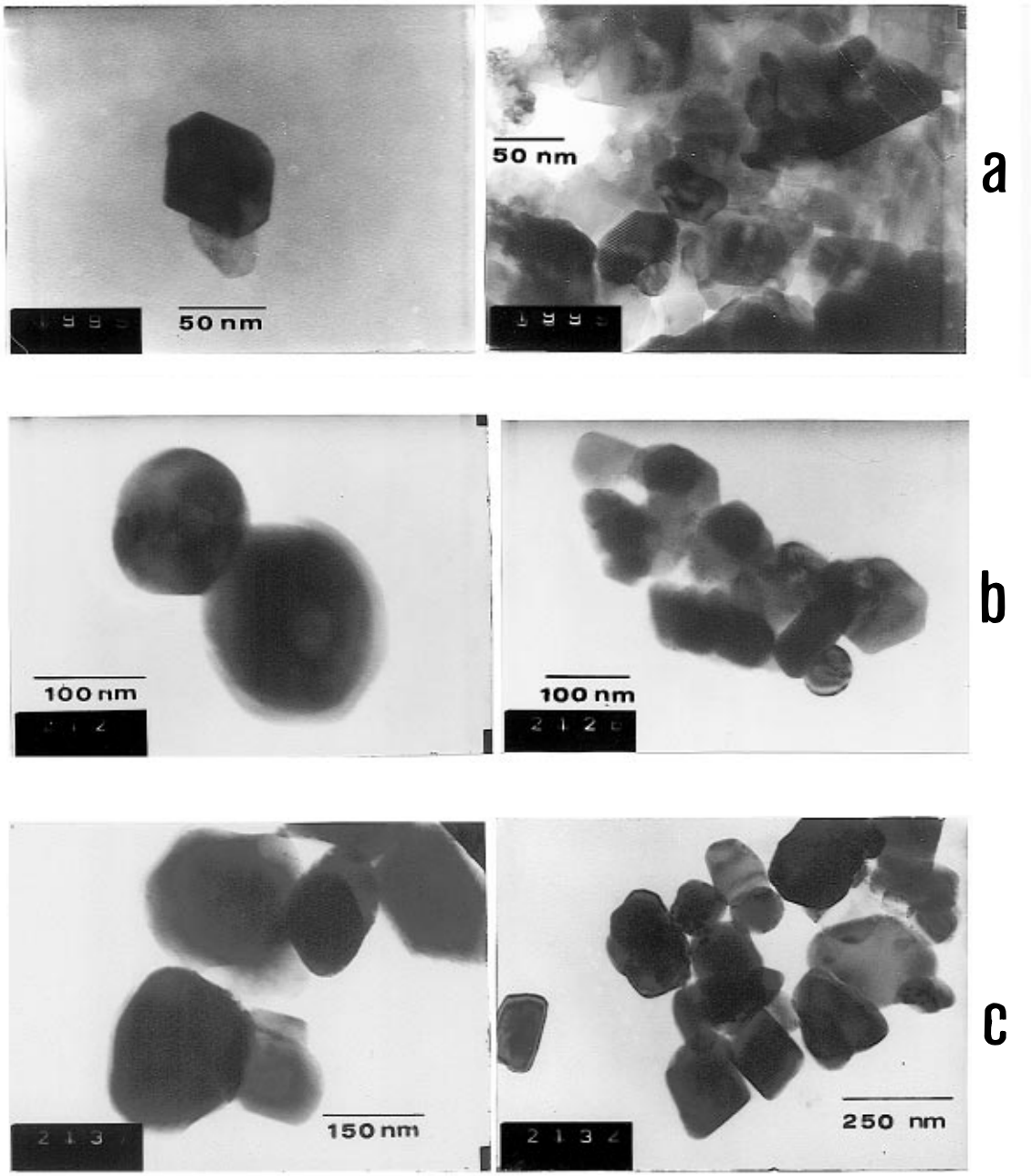

Figure 11. TEM micrographs on ex-citrate $LiCoO_2$ obtained at 400 °C for 20 h (a) and after further annealing at 600 °C for 5 h (b) and 25 h (c).

layers.[49,50] In the spectral range of CoO_2 vibrations, the IR spectrum of the ultrafine $LiCoO_2$ obtained at 400 °C shows four bands (Figure 13) as can be expected from the theoretical analysis for the D_{3d} group. Further calcination of ultrafine $LiCoO_2$ changes its IR spectrum. On increasing sintering temperature, the broad band at 500 cm^{-1} shifts to the higher wavenumbers and becomes narrower. The band at 614 cm^{-1} does not change its position up to 700 °C, whereupon it shifts to the lower wavenumbers. The other two bands are insensitive to additional annealing. These changes in CoO_2 layer dynamics, as well as the preservation of the trigonal lattice, can be explained by annihilation of extended defects during the sintering of the samples.

A problem arising out of the thermal decomposition of organic salts at low temperatures is the residual carbon in the oxide materials.[23] In an attempt to check the carbon content in ex-citrate $LiCoO_2$, EPR measurements were undertaken. The EPR spectrum of ex-citrate $LiCoO_2$ obtained at 400 °C displays a weak signal with $g = 2.001$ and a line width $\Delta H_{pp} = 1.26$ mT (Figure 14), which can be attributed to carbon. To determine the amount of carbon present in ex-citrate $LiCoO_2$, Figure 14 contains the EPR spectrum of the residual carbon obtained from the combustion of citric acid at 400 °C for 2 h. The comparison of the intensities of these ERP signals shows that the carbon content in ex-citrate $LiCoO_2$ is about 0.02 wt %. This low carbon content is similar to that found for the samples annealed up to 600 °C, whereas for the samples annealed at 800 °C, residual carbon is not detected by EPR.

Owing to the close chemical properties of cobalt and nickel, cobalt salts usually contain impurity nickel ions (less tha 0.5%). For diamagnetic $LiCoO_2$, nickel impuri-

(49) Moore, R. K.; White, W. B. *J. Am. Ceram. Soc.* **1970**, *53*, 679.
(50) Tarte, P.; Preudhomme, J. *Spectrochim. Acta* **1970**, *26A*, 747.

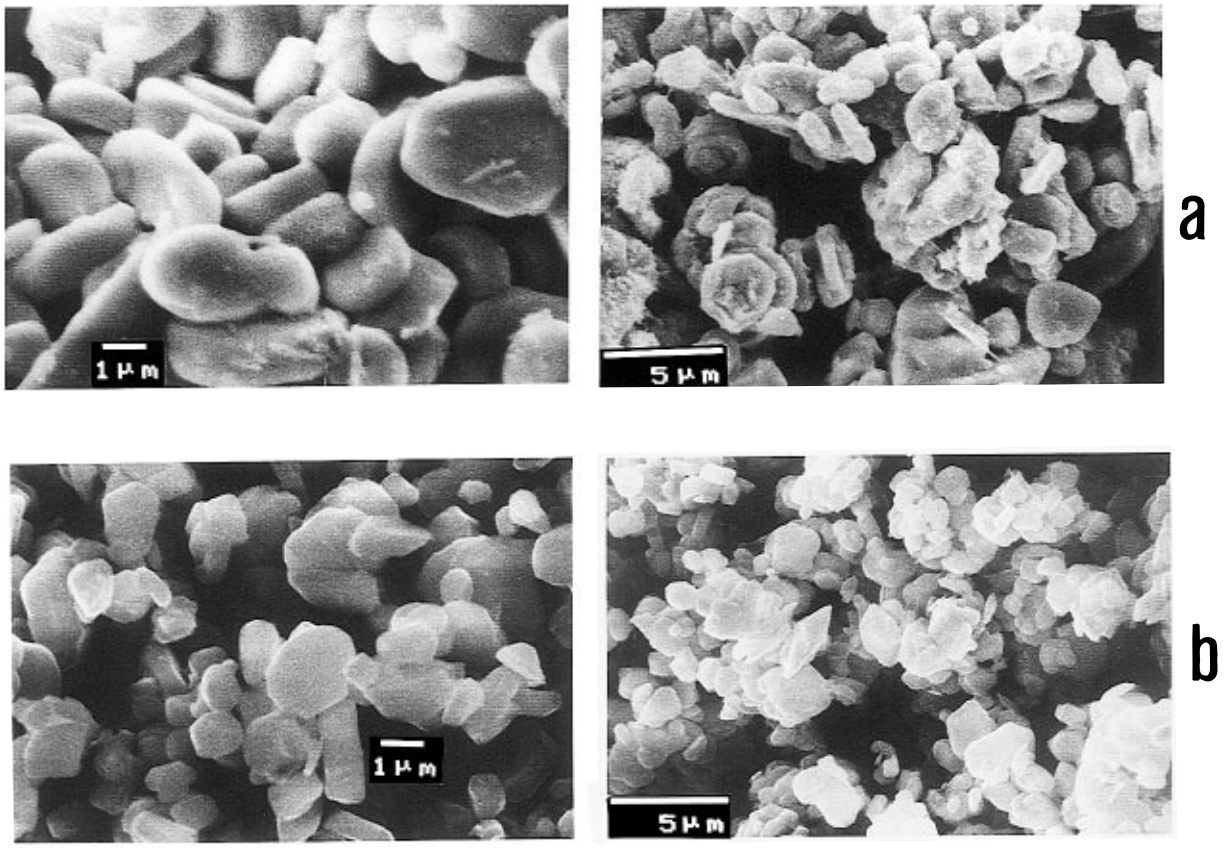

Figure 12. SEM micrographs of ex-citrate $LiCoO_2$ annealed at 800 °C for 10 h (a). For comparison, SEM micrographs of $LiCoO_2$ obtained by solid-state reaction between LiOH and Co_3O_4 at 800 °C for 24 h are also given (b).

Table 2. Annealing Temperature (*T*, °C) and Time (*t*, h), Specific Surface Area (*S*, m^2/g), Unit-Cell Parameters (*a* ± 0.0030 Å and *c* ± 0.020 Å) for Space Group *R*3*m* and *c*/*a* Ratio for Ex-Citrate $LiCoO_2$ Obtained at 400 °C for 20 h and after Further Annealing between 500 and 800 °C (*T*, °C) for 5−25 h (*t*, h)

T, °C	*t*, h	*S*, m^2/g	*a*, Å	*c*, Å	*c*/*a*
400	20	7	2.8160	14.021	4.979
500	5	7	2.8149	14.004	4.975
600	5	7	2.8143	14.007	4.977
600	25	4	2.8152	14.008	4.976
700	5	3	2.8150	13.992	4.971
800	5	1	2.8158	13.991	4.969
800	10	≤1	2.8150	13.997	4.972

ties give rise to an EPR signal with $g = 2.142$ due to low-spin Ni^{3+} (Figure 14). Recently, it was shown that impurity low-spin Ni^{3+} ions can be used as EPR probe in the CoO_2 slabs.[51] The impurity Ni^{3+} ions occupy two sites: (i) Ni^{3+} in trigonally distorted octahedra substituting isomorphically for the Co^{3+} ions in the CoO_2 layers; (ii) Ni^{3+} in tetragonally distorted octahedra related to some defect sites (surfaces) of the matrixes.[51] At $T > 30$ K, the EPR spectrum of Ni^{3+} ions displays the typical features of the dynamic Jahn−Teller effect: the thermally averaged Lorentzian line with $g = 2.142$ narrows with increasing registration temperature, and, between 170 and 220 K, the line width reaches its minimal value.[51] Table 3 shows the "temperature-independent" EPR line width ($\Delta H_{pp}°$) for impurity Ni^{3+} ions in ultrafine $LiCoO_2$ obtained at 400 °C, as well as for the samples calcined at 500, 600, 700, and 800 °C. As one can see, $\Delta H_{pp}°$ slightly decreases when the calcination temperature increases. Above 210 K, the Lorentzian line is broadened due to the spin−lattice relaxation processes (Figure 15). The experimentally observed dependence of the EPR line width on the

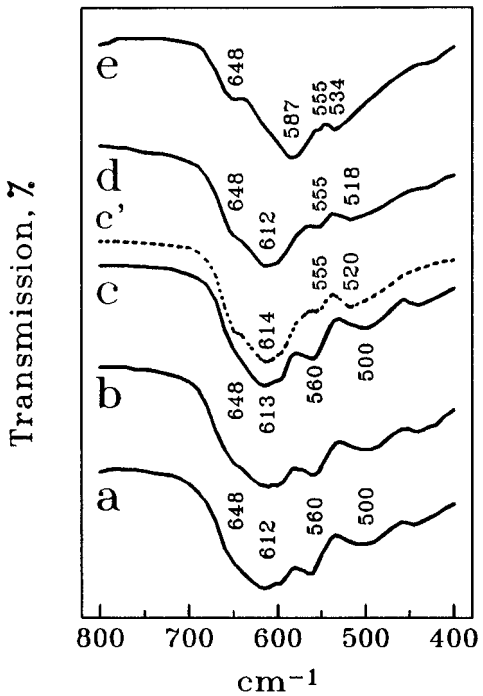

Figure 13. IR spectra of ex-citrate $LiCoO_2$ obtained at 400 °C for 20 h (a) and after further annealing for 5 h at 500 (b), 600 (c), 700 (d), and 800 °C (e). Spectrum (c′) was recorded after further annealing at 600 °C for 25 h. The spectra were recorded with KBr pellets.

(51) Angelov, S.; Friebel, C.; Zhecheva, E.; Stoyanova, R. *J. Phys. Chem. Solids* **1992**, *53*, 443.

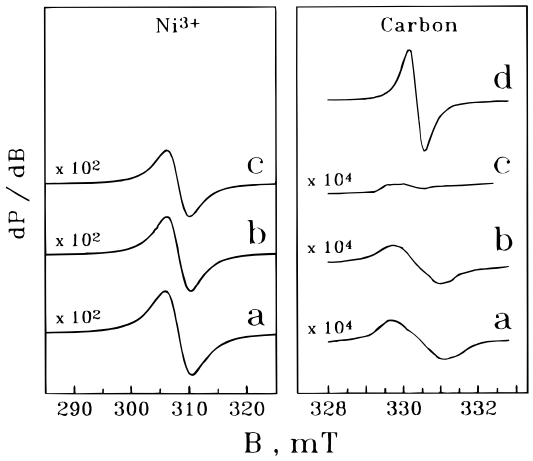

Figure 14. EPR spectra of ex-citrate $LiCoO_2$ obtained at 400 °C for 20 h (a) and after further annealing for 5 h at 600 (b) and 800 °C (c). The spectrum d corresponds to the residual carbon obtained by combustion of citric acid at 400 °C for 2 h.

Table 3. Temperature-Independent EPR Line Width ($\Delta H_{pp}°$, mT), $d(\Delta H_{pp} - \Delta H_{pp}°)/dT^2$ Coefficient ($b \pm 0.10$, mT/K²) and EPR Signal Intensity ($I \pm 0.2$, au) for Ex-Citrate $LiCoO_2$ Obtained at 400 °C and after Further Annealing between 500 and 800 °C (T, °C) for 5−25 h (t, h)

T, °C	t, h	$\Delta H_{pp}°$	$b \times 10^{-5}$	I
400	20	3.50	2.23	6.3
500	5	3.52	2.11	6.8
600	5	3.38	2.33	6.1
600	25	3.10	2.89	8.1
700	5	3.05	2.75	4.3
800	5	2.95	3.79	2.5
800	10	2.90	3.82	3.0

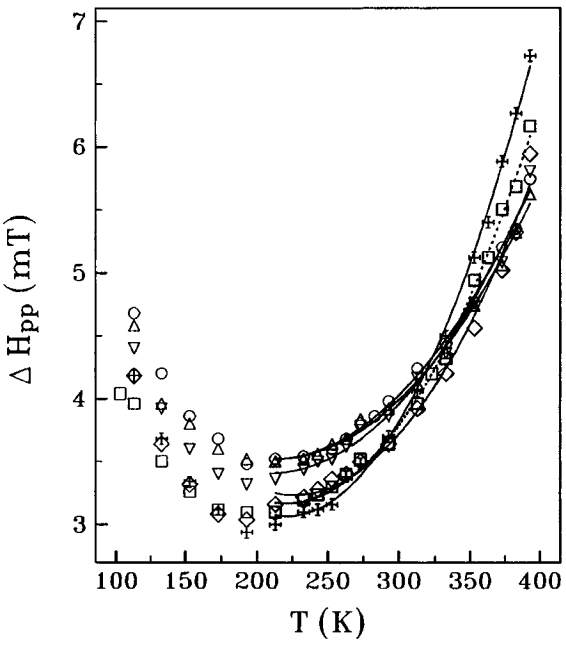

Figure 15. Temperature dependence of the EPR line width, ΔH_{pp}, for ex-citrate $LiCoO_2$ obtained at 400 °C for 20 h (○), and after further annealing for 5 h at 500 (△), 600 (▽), 700 (◇), and 800 °C (+). (□) Sample annealed at 600 °C for 25 h.

registration temperature is fitted with a quadratic function:

$$\Delta H_{pp} = \Delta H_{pp}° + \text{const} \times T^2 \qquad \text{at } T > 210 \text{ K} \quad (1)$$

The "T^2" broadening of the Lorentzian line is an indication that Ni^{3+} ions relax independently by Raman interactions with the phonon reservoir. The values of the $d(\Delta H_{pp} - \Delta H_{pp}°)/dT$ coefficient, which are reciprocal to the spin−lattice relaxation time, are given also in Table 3. A sharp decrease of the spin−lattice relaxation time of Ni^{3+} ions is observed for the samples heated above 600 °C, thus revealing changes in crystal lattice dynamics. Since the trigonal structure of $LiCoO_2$ is preserved during the sample sintering (Table 2) it can be inferred that the crystal lattice defects (most probably extended defects such as stacking faults, twinning, etc., which are typical for a layered lattice) will contribute mainly to the changes in crystal lattice dynamics. This is in a good accordance with the IR data concerning CoO_2 layer dynamics during sample annealing (Figure 13). In addition, the intensity of the EPR signal, which is proportional to the Ni^{3+} content, depends on the calcination temperature in the same way as the "temperature-independent" line width, $\Delta H_{pp}°$ (Table 3). The decreased amount of Ni^{3+} ions in the annealed samples can explain the narrowing of the "temperature-independent" EPR line width. In the case of statistical distribution of impurity Ni^{3+} ions in $LiCoO_2$ matrix, a quadratic dependence of the EPR line width on the spin amount must be expected: $\Delta H_{pp}^2 = \text{const} \times c$.[51,52] For the ex-citrate $LiCoO_2$ annealed at different temperatures, the quadratic dependence is not obeyed which indicates that the impurity Ni^{3+} ions are nonuniformly distributed. This result implies that the Ni^{3+} ions are localized mostly around the crystal lattice defects (extended defects). During sample annealing, the annihilation of the crystal lattice defects will cause a segregation of these Ni^{3+}, thus making them EPR "silent" due to the magnetic dipole−dipole interactions (Table 3). The appearance of extended defects in ultrafine ex-citrate $LiCoO_2$ with $c/a \cong 4.97$ would be of great importance for the lithium transport and, consequently, for the cell performance.

Electrochemical Measurements. Figure 16 shows the first cycle voltammograms of lithium anode cells using four selected ex-citrate $LiCoO_2$ samples as positive electrode active material. In these plots, the main charge peak occurs at ca. 4.00 V for samples prepared at 600 and 800 °C, while a slightly lower value (3.97 V) was observed for the lower temperature sample. Nevertheless, these differences are not so notorious such as those reported for LT and HT preparations of $LiCoO_2$ by conventional procedures.[10] Moreover, these authors found a two-step lithium extraction process between 3.6 and 4.0 V which was attributed to the removal of lithium ions from the 3a octahedral sites of the structure followed by the removal of further lithium ions and the formation of a second phase with lithium ions in both tetrahedral and octahedral sites. These effects are not resolved in the voltammograms of ex-citrate samples. In addition, the current relaxation plots for the voltage steps of the SPES experiment in the 3.6−4.0 V range, such as that shown in Figure 17 for the sample obtained at 400 °C, show evidence for a single lithium ion diffusion plus electron-release process during cell charge which involves energetically equivalent sites. It should also be noted that the shape of the curves obtained at the different synthesis temperature do not differ in the

(52) Van Vleck, J. H. *Phys. Rev.* **1948**, *73*, 1249.

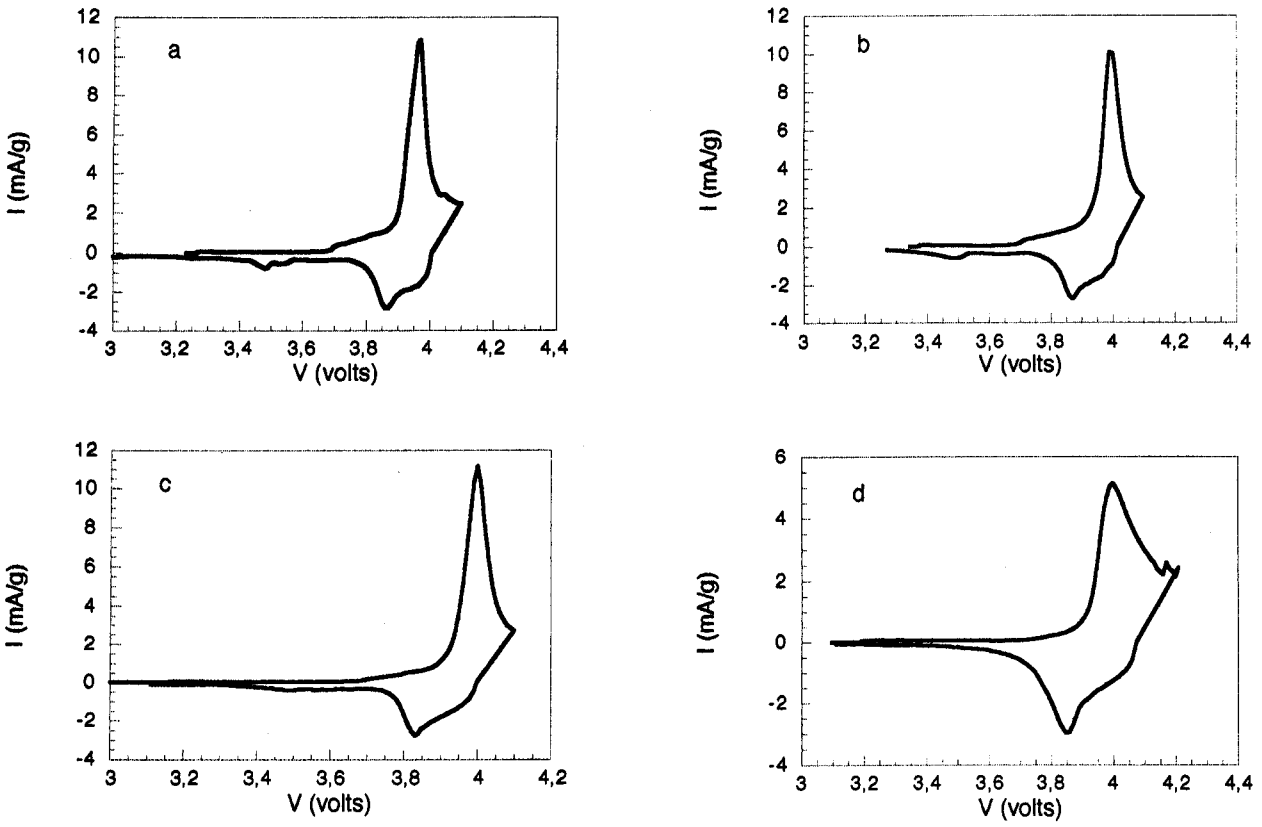

Figure 16. Step potential electrochemical spectroscopy voltammograms vs a pure lithium anode of ex-citrate $LiCoO_2$ samples obtained at (a) 400 °C, 20 h, (b) 600 °C, 5 h, (c) 600 °C, 25 h, and (d) 800 °C, 10 h.

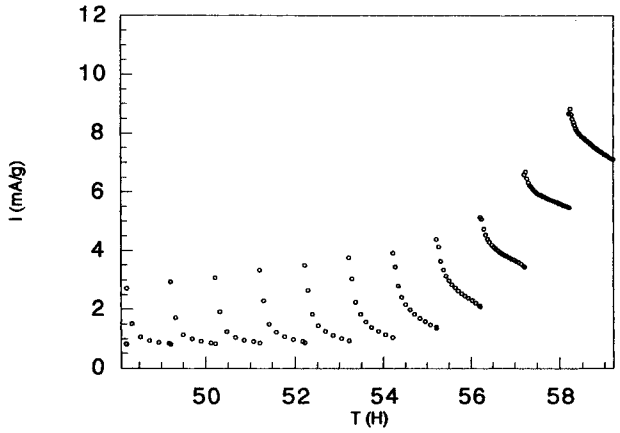

Figure 17. Current relaxation for potential steps in the 3.6–4.0 V interval during the charge of a lithium cell using the ex-citrate $LiCoO_2$ sample obtained at 400 °C as cathode material.

main oxidation and reduction peaks. These effects are indicative of a larger departure from the spinel structure in ex-citrate samples prepared at 400 °C than in the "conventional" LT samples.[10]

Recently, Yazami et al.[19] studied ex-acetate $LiCoO_2$ samples, in which the voltage of the oxidation and reduction peaks showed little changes with the synthesis temperature. Similarly, the difference between both voltage values changed smoothly with preparation temperature (0.06 V for LT and 0.10 V for HT preparations). In contrast, the difference in peak voltage for the ex-citrate sample obtained at higher temperature (0.15 V for 800 °C) is larger than that found in the 400 °C sample (0.11 V). On the other hand, the peak intensity of the main reduction and oxidation peaks decreases significantly on increasing the synthesis temperature of the ex-citrate samples. In addition, the intensity ratio between the cathodic and anodic peaks is closer to unity and the main peaks are more broadened on increasing the preparation temperature. These broadening effects may be a consequence of the increase in particle size observed with the preparation temperature, which imply longer periods of slow diffusion of the lithium ions in the larger particles of the samples prepared at higher temperatures.[19]

Other features of the voltammograms in Figure 16 include the presence of a charge peak at ca. 4.15 V with the corresponding discharge effect that occurs as a shoulder of the main reduction peak at ca. 4 V. This effect is clearly resolved for the sample prepared at 800 °C, and its nature may be related to an order–disorder transition such as those observed in the incremental capacity vs voltage plots reported by Reimers and Dahn[16] in samples prepared from lithium hydroxide and cobalt carbonate mixtures at 850 °C. An additional peak at ca. 4.2 V starts to be visible in Figure 16d. Finally, a low-intensity discharge peak is observed at ca. 3.5 V in which the intensity decreases with synthesis temperature. This effect has been ascribed to a cation disorder in the structure and was also found by Yazami et al.[19] ex-acetate solids.

On the other hand, the capacity of these materials in constant current experiments was tested during the first four cycles (Figure 18). Cell capacity increases significantly with the preparation temperature of the cathode material, particularly between 600 and 800 °C, even after 25 h treatments. However, the loss of capacity during the first four cycles in samples prepared at 600 and 400 °C is less marked than in materials obtained

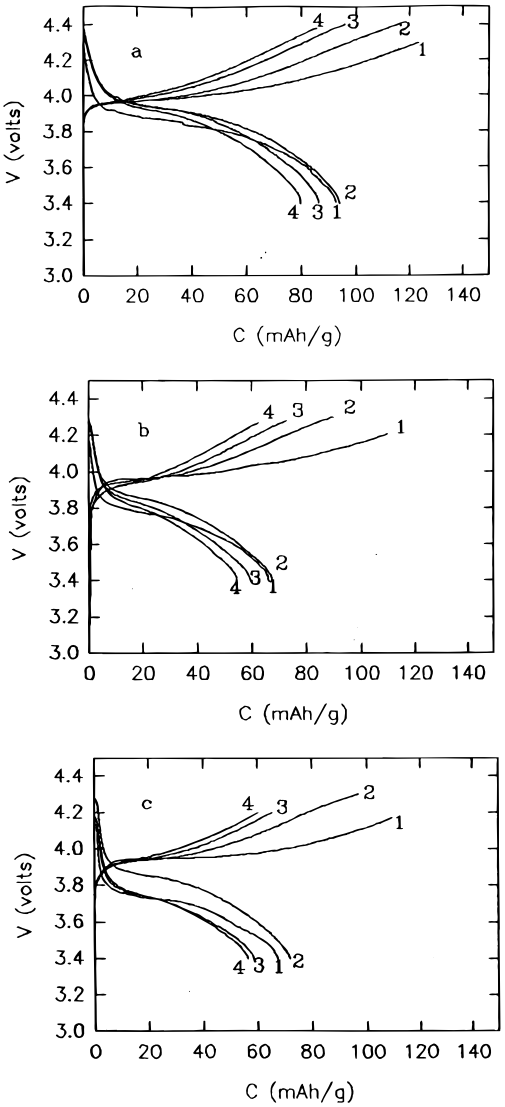

Figure 18. Galvanostatic cycling at C/50 of lithium cells using ex-citrate $LiCoO_2$ samples obtained at (a) 800 °C, 10 h, (b) 600 °C, 25 h, and (c) 400 °C, 20 h.

by other preparative procedures. Thus, LT-$LiCoO_2$ prepared from Li_2CO_3 and $CoCO_3$ at 400 °C for 5 days shows a significant loss of capacity during cycling, reaching capacities lower than 20 mA h/g after the first four cycles.[6] For ex-citrate samples cycled at a similar current density (ca. 0.15 mA/cm^2) cell capacities higher than 50 mA h/g were found after the fourth cycle (Figure 18c).

Conclusions

In concentrated lithium−cobalt citrate solutions with Co/citrate = 1/1 and 1/2, the predominant species at pH = 7 are $[Co(C_6H_5O_7)]^-$ and $[Co(C_6H_5O_7)_2]^{4-}$ complexes. Ethanol dehydration of the two types of solution leads to the formation of homogeneous $LiCoC_6H_5O_7 \cdot 5H_2O$ and $(NH_4)_3LiCo(C_6H_5O_7)_2$ compositions, where Co^{2+} ions are complexed by one and two triionized citrates, respectively, the Li^+ ions serve as counterions. Lithium−cobalt citrate salts are appropriate precursors for the low-temperature preparation of $LiCoO_2$. At 400 °C, thermal decomposition of $LiCoC_6H_5O_7 \cdot 5H_2O$ yields a mixture of pseudo-spinel and rhombohedral $LiCoO_2$. From $(NH_4)_3LiCo(C_6H_5O_7)_2$, monophase powders of rhombohedral $LiCoO_2$ were obtained at 400 °C, which consist of hexagonal individual particles with a diameter of 80−120 nm. These products contain negligible amounts of residual carbon (about 0.02 wt %). Cyclic voltammograms of rhombohedral $LiCoO_2$ showed little changes in the main oxidation and reduction peaks with preparation temperature. The loss of capacity during the first four cycles is less marked in ex-citrate samples prepared at 400 °C than in materials obtained by preparative procedures different from the precursor method. These solids have interesting possibilities of application in advanced battery technology.

Acknowledgment. The authors are indebted to EC for financial support (Contract JOU2-CT93-0326, Supplementary Agreement ERBCIPD-CT94-0501). The LQI group also thanks the financial support from CICYT (MAT94-1155-CE).

CM960009T